10

Rapid #: -2537911

Ariel
IP: 18.51.0.167

Status	Rapid Code	Branch Name	Start Date
Pending	DLM	Main Library	5/6/2009 8:16:46 AM

CALL #: **TA365 .J59**
LOCATION: **DLM :: Main Library :: MAIN_GEN**

E

TYPE: Article CC:CCG
JOURNAL TITLE: Journal of computational acoustics
USER JOURNAL TITLE: Journal of computational acoustics
DLM CATALOG TITLE: Journal of computational acoustics.
ARTICLE TITLE: THREE-DIMENSIONAL ACOUSTICS EFFECTS IN THE ASIAEX SCS EXPERIMENT
ARTICLE AUTHOR: Chiu
VOLUME: 17
ISSUE: 1
MONTH:
YEAR: 2009
PAGES: 11-27
ISSN: 0218-396X
OCLC #: 29352806
CROSS REFERENCE ID: 149656
VERIFIED:

BORROWER: **MYG :: Main Library**
PATRON: **Leslie,Wayne**

PATRON ID:
PATRON ADDRESS:
PATRON PHONE:
PATRON FAX:
PATRON E-MAIL: wgleslie@mit.edu
PATRON DEPT: MECHENG
PATRON STATUS: RS
PATRON NOTES:

Journal of Computational Acoustics, Vol. 17, No. 1 (2009) 11–27

INTERNATIONAL ASSOCIATION
FOR MATHEMATICS AND
COMPUTERS IN SIMULATION

THREE-DIMENSIONAL ACOUSTICS EFFECTS IN THE ASIAEX SCS EXPERIMENT

YUNG-SHENG CHIU*, YUAN-YING CHANG*, LI-WEN HSIEH*,
MEI-CHUN YUAN† and CHI-FANG CHEN*,‡

*Department of Engineering Science and Ocean Engineering
National Taiwan University, Taipei, 106, Taiwan, R.O.C

†Department of Information Management
Meiho Institute of Technology, Taiwan, R.O.C

‡chifang@ntu.edu.tw

Received 17 September 2007
Revised 23 January 2008

A three-dimensional (3D) ocean environment is assimilated with measured ocean data in the ASIAEX SCS (Asian Seas International Acoustics EXperiment, South China Sea) experiment. The experiment site is characterized as an active internal wave propagation region along the Northwestern shelf break of the South China Sea. Three-dimensional acoustics effects in the area are studied using FOR3DW, a wide-angle version of the parabolic equation code FOR3D (a Finite difference solution, an Ordinary differential equation, and Rational function approximations for solving 3D problems), and MOS3DPEF (MOdal Spectrum analysis based on 3D PE Field). The TL comparison between Nx2D and 3D calculations are shown to demonstrate the 3D effects. Variations in topography of the shelf break and in the water column due to the internal waves cause the 3D effects in the acoustic field. The intercomparison of the importance of bottom steering 3D effects and nonlinear internal wave refraction 3D effects is therefore proposed to realize which possesses the major part of the 3D effects. Also, 3D modal analysis results show that the nonlinear internal wave front causes severe horizontal refraction for higher modes.

Keywords: ASIAEX SCS; FOR3D; MOS3DPEF; internal wave; parabolic equation; 3D effect; underwater sound propagation.

1. Introduction

Three-dimensional (3D) effects on underwater acoustic propagation have been frequently reported.[1–6] The major causes for the 3D effects are variations in azimuth of bottom topography and/or water column properties.[7–11] The ASIAEX SCS site is of a similar nature, in that both bathymetry and horizontally anisotropic water column properties contribute to horizontal refraction of energy. This paper demonstrates the 3D effects of acoustic propagation at the experimental site using assimilated ocean data. The intercomparison of the importance of bottom steering 3D effects and nonlinear internal wave refraction 3D effects is also proposed to realize which possesses the major part of the 3D effects.

This paper is organized as follows. Section 2 describes the ocean environment assimilated with measured mooring data. Section 3 presents the detection scheme for 3D effects in

numerical simulation for 3D propagation runs. Section 4 discusses the numerical test cases and transmission loss calculations. Section 5 presents a study of 3D modal analysis and the results. The concluding remarks are stated in Sec. 6.

2. Construction of a Data-Driven 3D Ocean Sound Speed Model

During the experiment, the environment was widely surveyed, including bathymetry and mooring data.[12] To the mesoscale and the internal tide scale, the measured data are enough to reconstruct the ocean environment. However, to the soliton scale, the ocean temperature data are sparsely sampled in horizontal space comparing with vertical direction making it difficult to reconstruct the ocean environment directly from the limited data sets for investigation of 3D effects. More specifically, without Kuroshio intrusions the mesoscale was large in 2001 and was well sampled by the moorings. The internal tide scale, which is about 40 km, was also sampled adequately by the moorings. Nevertheless, the solitons, or the nonlinear internal waves, observed had around 100–400 m individual wave scales and hence were aliased by the moorings. Therefore, some additional information is required to supplement the oceanographic data. This creates the need for an oceanographic model of the soliton component. In this section, we discuss the bathymetry of the region and the reconstruction of the ocean environment based on observations and measurements.

The bathymetry of the area is shown in Fig. 1, along with a 2D bathymetric contour representation of the moored instruments. Compiling the bathymetric data from the five cruises, OR3-651 (the 651st voyage of Taiwanese Oceanographic Research vessel 3), OR1-609, OR1-610, OR1-611, and OR1-677, we established a database with grid spacing of 500 m using the results provided by NCOR (National Center for Ocean Research) of Taiwan. From the database, we draw the bathymetric contour lines for two fan-like regions that will be considered for acoustic modeling (Fig. 1), corresponding to deep (across-shelf) and shallow (along-shelf) acoustic propagation tracks, respectively. It is seen that both the along-shelf (shallow source) and across-shelf (deep source) paths contain some highly irregular bathymetry, which is typical of this region. It is clear from the figure that the bottom is relatively flat to the north, followed by a cliff-like transition in the middle of the area, and a gentle slope to the south.

Owing to the sparseness of the three deployed environmental mooring at water depth 120, 200, and 350 m mooring data points (env-120, env-200, and env-350) as shown in Fig. 1, it was found necessary to make use of additional information to sample the 3D environment for acoustic propagation studies. In general, there was an important aspect of the internal wave field in this area, namely the three distinct periods of internal wave activity. From May 2 to May 6, there was a strong diurnal internal tide component, but few solitary wave activities. From May 6 to May 14, the semidiurnal internal tidal component was more pronounced and there also presented a substantial soliton field. After May 14 till 18, the conditions reverted to the first period. We focus on May 4 (of the first period, named internal tide period) and May 8 (of the second period, named nonlinear internal wave activity or the solitary wave activity).

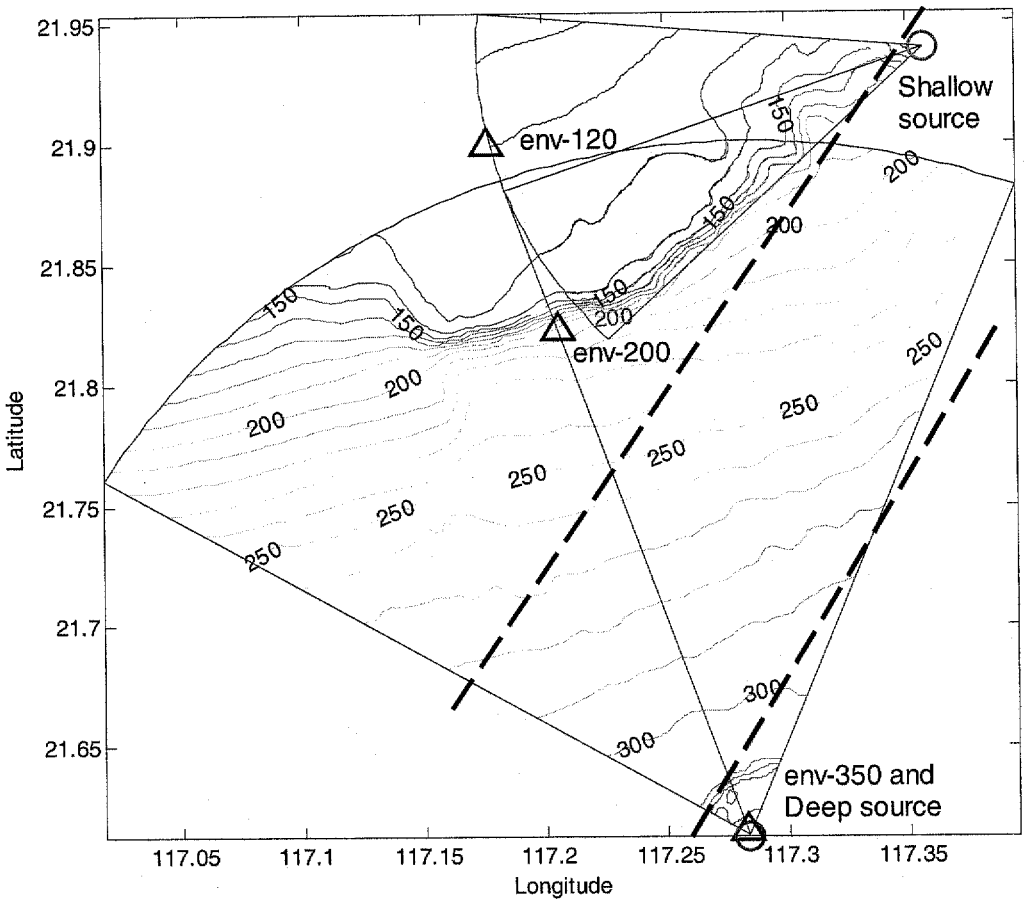

Fig. 1. Schematics of investigation area with sources and environment moorings locations marked on the bathymetric contour. The dashed lines denote the nonlinear internal wave crest.

From satellite images of the ASIAEX SCS site, it was found that the internal wave crest was nearly linear as it crossed the acoustic transmission tracks. An example is shown in Fig. 2, which was taken around 22:15 on 5 May 2001 provided by NRL. One can also estimate the internal wave propagation direction from the images. With the additional information provided by the environment mooring data, the propagation direction and speed can be calculated more accurately.[13]

From the observations, we have made the following fundamental assumptions. First, we assume that the internal waves propagating in a plane waveform without changing its direction between env-350 and env-120, so that one sound speed profile can be applied to any points on the track that is perpendicular to the propagation direction of internal waves. Second, we have considered the internal waves propagating at an averaged constant speed between env-350 and env-120 to simplify the problem.

However, these two assumptions do not valid for long range such as over 50 km near the shore. As seen in Fig. 2, it shows that as the propagation direction of the internal waves changes, their speeds change as well.[13] The internal waves changed its direction gradually

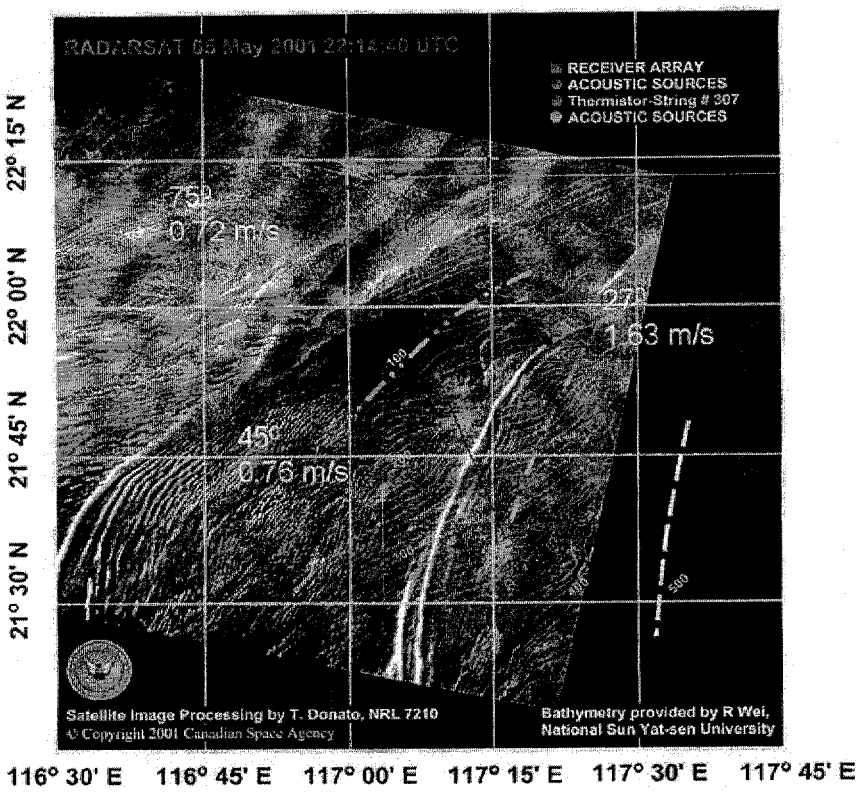

Fig. 2. Sample satellite image covering the experiment site taken on May 5th. Four dashed lines indicate the internal waves crests with some of the estimated direction and speed noted beside.

from westward to northward over 100 km. In addition, the waves propagate faster in deeper region and slow down near the shore. Owing to the shoaling of the water depth, the internal waves vary more rapidly while moving up to the shelf. Since the ranges of our cases are both less than 35 km, the assumptions are still acceptable. In other words, the leading edge of the nonlinear wave is probably close to a plane wave, but the later waves in the train are probably less planar. Also, the wave speeds for various waves in a wave group vary, i.e. the waves are slightly dispersive so that the constant velocity assumption for the whole group is somewhat erroneous.

Using the time series for the mooring data at the three locations shown in Fig. 1, as well as the assumptions stated above, the temperature profile was reconstructed over the investigation area in the following manner. First from the satellite image, the propagation angles are known as 297° for the deep region and 315° for the shallow region. Then from the mooring data on May 5 at env-120 and env-350 and the distance between them, we can calculate the average velocity of internal waves that is 1.39 m/s to the south. Similarly, we can also get the velocity 0.76 m/s to the east by using the mooring data May 5 at env-120 and env-200. Second, we transformed the temperature data from time versus depth to range versus depth, i.e. a 2D (r, z) profile, by using the propagation angles and the calculated wave speeds. We can straightly extend the profile along the internal wave crest that assumed

normal to the propagation direction. Thus, a 3D environment was reconstructed in a box area whose size is dependent on the length of the data recorded and as wide as was needed for the acoustic analysis. With this assimilated environment, a computational domain is defined for acoustic simulation studies.

Note that because of the difficulty in identifying the advent of internal waves at each mooring, there may be some errors in the calculated wave speed. Although this 3D environment is very simple to deal with, there should be some improvements on it.

3. Detection of 3D Effects

In this section, first the equations describing 3D, Nx2D, and 2D acoustic propagation are stated.[1] Then we describe the scheme for characterizing 3D effects from our calculation.

The corresponding equations for the far-field wave equation in cylindrical coordinates take the following forms. It can be easily seen that the 2D case is a special case of Nx2D, and the Nx2D case is a special case of 3D.

3D formulation:

$$u_{rr} + 2ik_0u_r + u_{zz} + \frac{1}{r^2}u_{\theta\theta} + k_0^2[n^2(r,\theta,z) - 1]u = 0. \tag{1}$$

Nx2D formulation:

$$u_{rr} + 2ik_0u_r + u_{zz} + k_0^2[n^2(r,\theta,z) - 1]u = 0. \tag{2}$$

2D formulation:

$$u_{rr} + 2ik_0u_r + u_{zz} + k_0^2[n^2(r,z) - 1]u = 0. \tag{3}$$

The 3D case with θ coupling can be interpreted as admitting both horizontal refraction and net energy transfer between adjacent vertical (r–z) planes. Both the amplitude and phase of the acoustic field can vary with θ as a result of the horizontal refraction of wavefronts because the index of refraction is a function of θ.

The Nx2D case does not include azimuthal coupling, and no net energy is exchanged between adjacent vertical planes as the acoustic field propagates. This can be revealed by checking the constancy of the depth average of acoustic energy (DAAE) along range direction.

In the 2D case, there is no variation of the acoustic field with θ, which would also be no variation either in a mean wavefront. This physical situation is one that has no horizontal refraction.

In this paper, we assumed that 3D effects come mainly from two sources: one is the variation of the water depth, i.e. the bathymetry; the other corresponds to the sound speed

perturbations caused by the internal wave packet. Note that fronts, when present, also can give very strong 3D behavior. The SCS in 2001 just did not happen to have one. To reveal the effects due to bathymetry, one can use a constant or averaged sound speed profile, i.e. a range-independent profile throughout the entire region of interest, and compare the results of 3D calculation with Nx2D calculation. We consider the following equation:

$$\Delta TL_B = TL_{B3} - TL_{B2}, \tag{4}$$

where TL is the calculated transmission loss, subscript B stands for bathymetry effects, and subscript 3 and 2 represent 3D and Nx2D, respectively.

It is straightforward to apply a similar approach for observing the effects caused by the water column sound speed variations, using a flat bottom with a varying sound speed profile. This leads to the expression

$$\Delta TL_W = TL_{W3} - TL_{W2}, \tag{5}$$

where subscript W stands for water column changes effect. However, (5) is not the case presented in this paper since at the ASIAEX site, the bathymetry variation exists while the water column sound speed varies with time. Rather, it is of interest to study the effects that the variations in water column sound speed will have on a calm ocean. Therefore, a fully range-dependent environment is first considered in order to describe its contribution to 3D effects:

$$\Delta TL_{(B\cup W)} = TL_{(B\cup W)3} - TL_{(B\cup W)2}, \tag{6}$$

and then "subtract" those contributions from the bathymetry component:

$$\Delta TL_{(B\cup W)-B} = \Delta TL_{(B\cup W)} - \Delta TL_B. \tag{7}$$

Since the subtraction is carried out on a dB scale, such subtraction in (7) does not directly give the effects due to the water column changes, but describes how much the combination effects compare with those due only to variations in the bathymetry. This is also the reason we use the symbol $\cup$ here instead of $+$ to emphasize that the two effects are coupled here rather than linearly combined together.

4. Transmission Loss Calculations

Among the existing 3D PE codes,[14] we have adopted the wide-angled version of FOR3D,[2] a model that has the capability of handling 3D azimuthal variation effects, i.e. θ coupling, to perform all the computations for the test cases presented in this paper.

The computations discussed below involve several scenarios. Referring to the experiment configuration in Fig. 1, we have a shallow 400 Hz source to the east (this case is denoted by S400, shallow) while to the south in deeper water, are 224 and 400 Hz sources (this case will be denoted by D224 and D400). The actual bathymetry is applied to all cases, though three different assimilated sound speed profiles for cases S and D were used.

Table 1. Computation configuration.

Source Location	Investigation Area	Frequency (Hz)
Deep at 331.3 m		224
E117.2837, N21.6129	32 km by 80° (341° ± 40°)	400
Shallow at 99.7 m		
E117.3573, N21.9392	19 km by 50° (250° ± 25°)	400

In S cases, one profile is taken at 11:34 on May 4 when the internal tide is located at the middle of the acoustic transmission track. Another is taken at 12:14 on May 8 when the nonlinear internal waves were between the source and the receiver. In addition, a mean profile is taken by averaging the complete temperature data set from April 22 to May 17. As for the D cases, the events are the same except for the corresponding time at 09:42 on May 4 and 10:14 on May 8. That is, for the water column, we have two 3D range-dependent and one range-independent environment as a background calculation for comparison.

In summary, there are nine cases in our investigation of 3D effects. Some parameters of the computation are summarized in Table 1. The results for the D cases are given first, followed by the S cases.

In Fig. 3(a), plots in the first row show the sound speed profile along the deep acoustic propagation track that is the centerline of our calculation area. The scale of the sound speed is 1500–1541 m/s and this scale applies to all the other sound speed plots. From left to right, they are designated as the internal tide profile observed on May 4, the mean profile averaged over whole experiment period, and the nonlinear internal waves profile observed on May 8. The second and fourth rows are the transmission loss results for the D224 case, whereas the other two rows correspond to the loss for the D400 case. The second and third rows represent transmission loss from 3D calculations with corresponding environments shown in the top row. The lowest two rows correspond to comparisons calculated from (4) and (7) with different environments, respectively.

The first row in Fig. 3(b) shows the sound speed distribution at a depth of 100 m from which the sharp changes due to internal waves are evident. The sequence of the results in each row and column is the same as in Fig. 3(a) except that now the results are drawn at a specified depth, and top viewed on a $r - \theta$ plane. Similar to the deep cases, Figs. 4(a) and 4(b) show the results of shallow case. The fixed depths shown in Fig. 4(b) are chosen at 70 m.

For the deep source cases, the range of TL shown in the figure is 50–100 dB, whereas for TL difference it is ±9 dB. For shallow source cases, the range of TL shown in the figure is 45–95 dB, whereas for TL difference it is ±15 dB.

Table 2 lists all the quantities calculated by (4), (6), and (7) from the results along the two propagation tracks and on specific horizontal planes at fixed depths. They, results of (4) and (7) correspond to the TL difference plots in Figs. 3 and 4. The mean square TL differences are 2–5 dB, which is 1.5 times larger in shallow case relative to the deep cases.

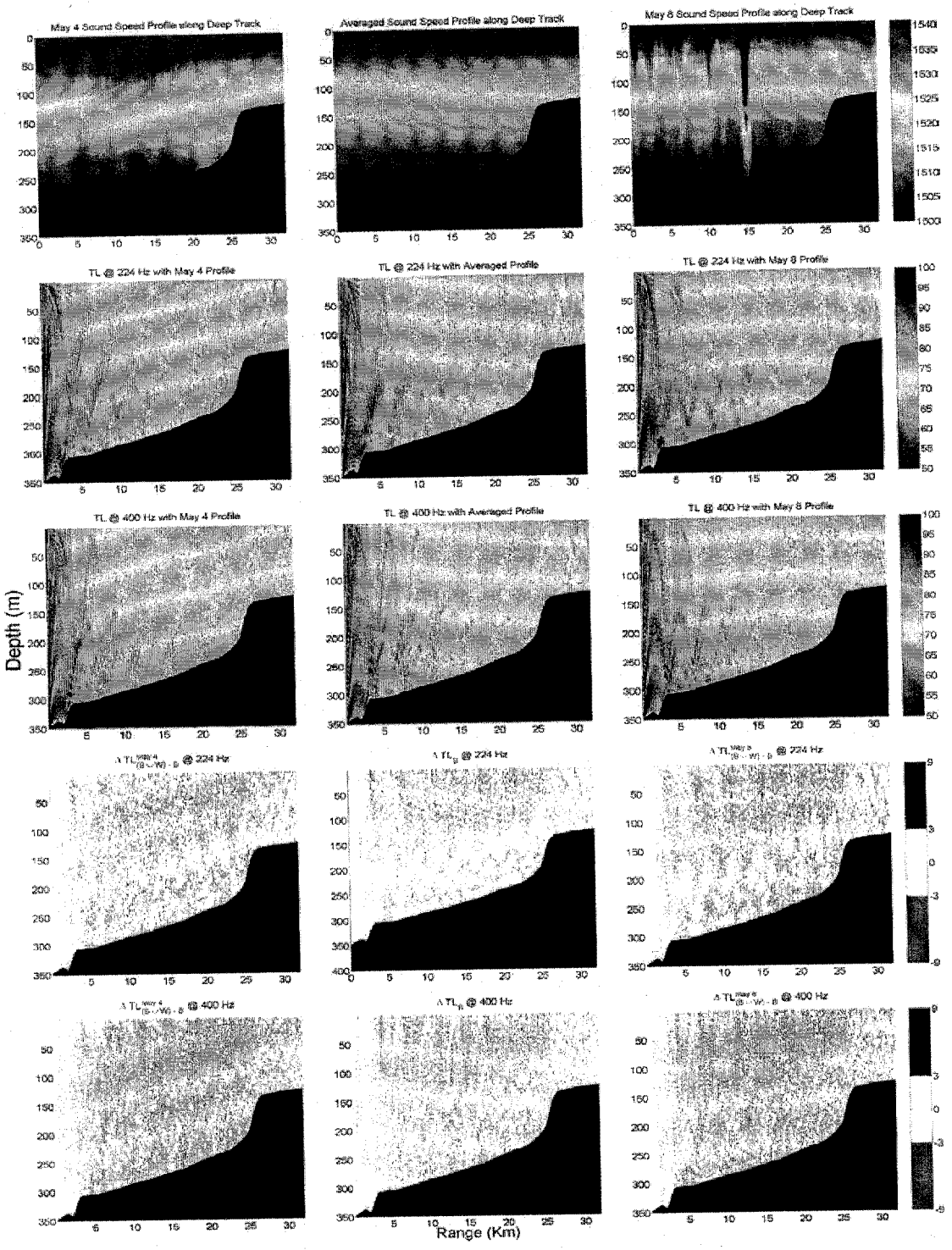

(a)

Fig. 3. Plots from top to bottom are the environment, TL results and differences of D224 and D400 cases, whereas from left to right corresponding to profiles on May 4, averaged, and on May 8. All the data are plotted (a) along the acoustic transmission track and (b) at 100 m depth.

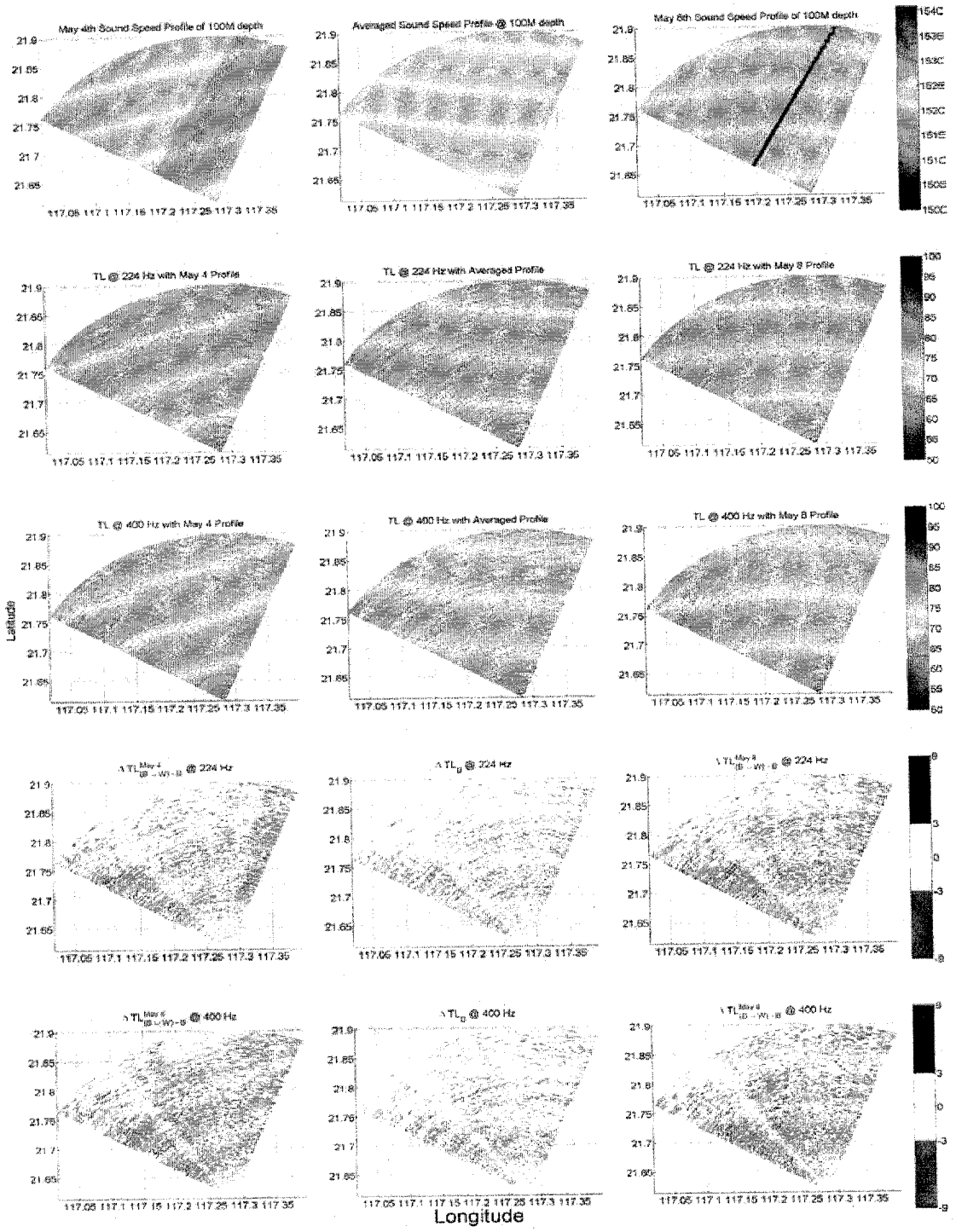

(b)

Fig. 3. (*Continued*)

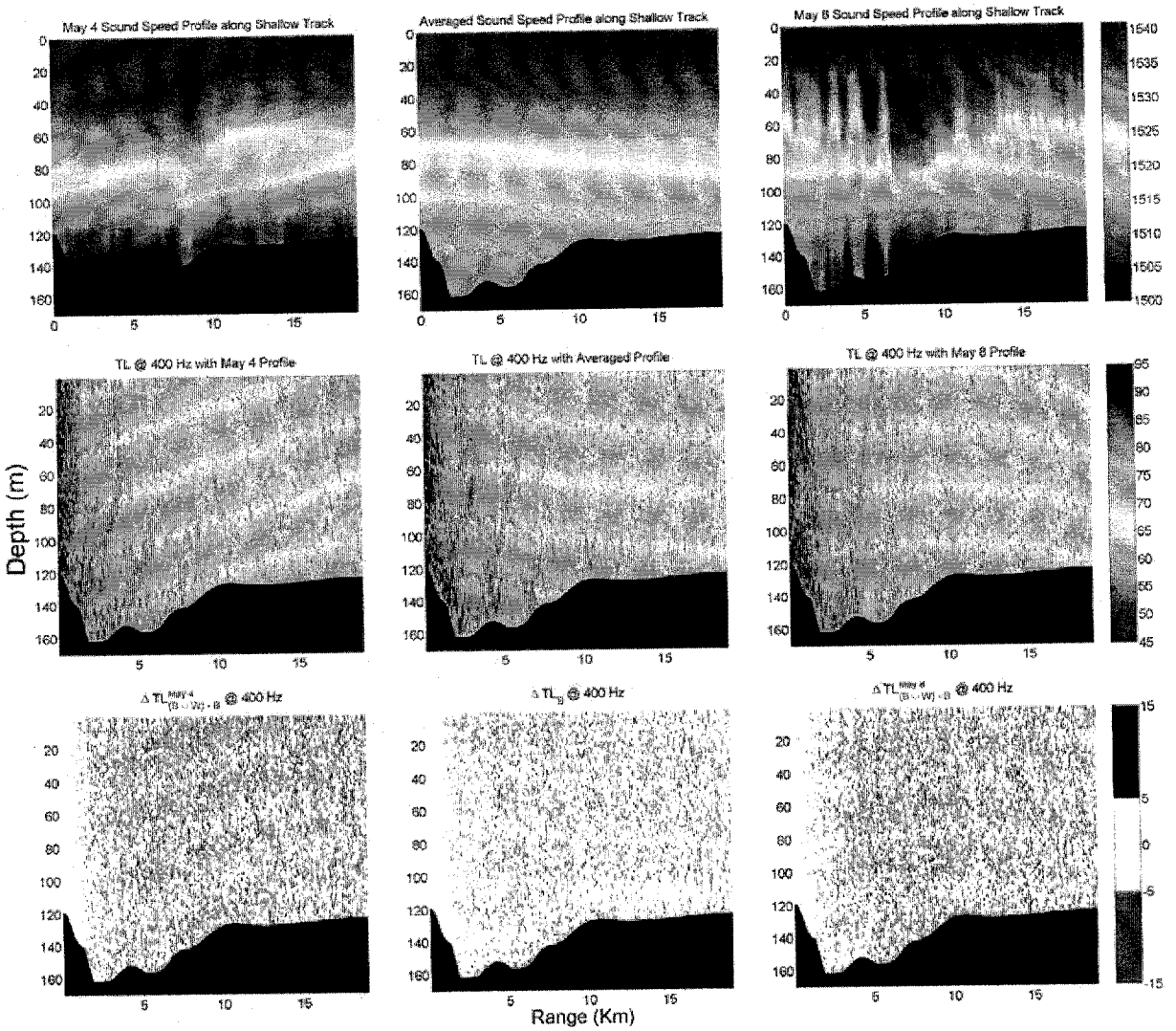

(a)

Fig. 4. Plots from top to bottom are the environment, TL results and differences of S400 cases, whereas from left to right corresponding to profiles on May 4, averaged, and on May 8. All the data are plotted (a) along the acoustic transmission track and (b) at 70 m depth.

Comparing case D224 to D400 across frequency, there is no distinguishable difference both in the results given by (4) and (6). However, when we apply (7), one does see a difference between the two cases. Comparison between the results by (6) and (7) shows larger difference from (7), this arises from a phase shift in the TL distributions. Three-dimensional effects due to bathymetry and nonlinear internal wave perturbation are about the same order as 3D effect due to bathymetry alone, whereas 3D effects due to nonlinear internal wave perturbation subtracted from the bathymetric effect are largest among all, say, 1–2 dB larger.

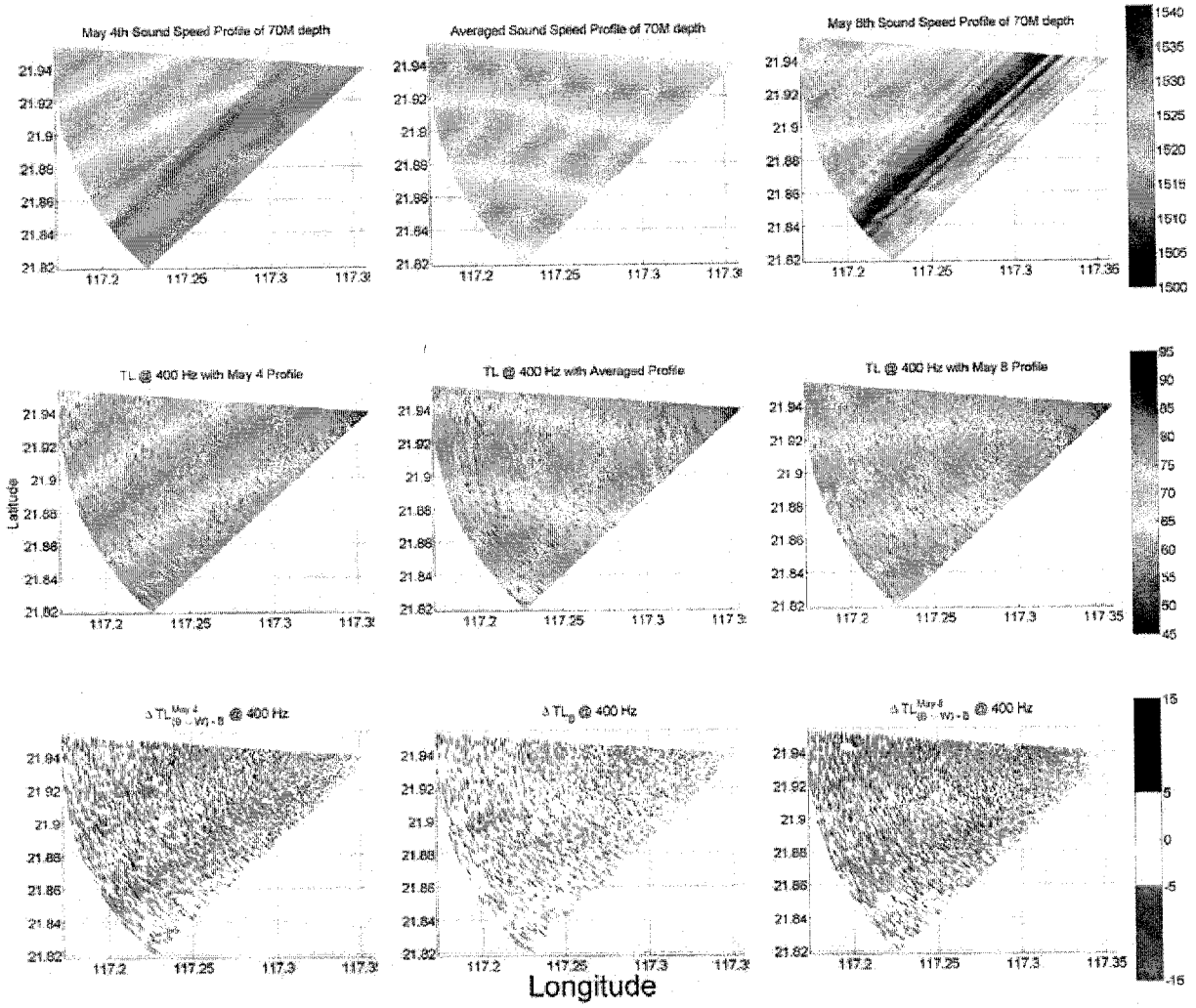

(b)

Fig. 4. (*Continued*)

Table 2. Statistics of TL differences.

Mean Square Difference (dB)		ΔTL_B (4)	May 4		May 8	
			$\Delta TL_{(B\cup W)-B}$ (7)	$\Delta TL_{(B\cup W)}$ (6)	$\Delta TL_{(B\cup W)-B}$ (7)	$\Delta TL_{(B\cup W)}$ (6)
D224	Track	2.4	2.7	2.5	2.6	2.3
	100 m	2.1	2.6	2.0	2.8	2.2
D400	Track	2.2	3.0	2.3	3.0	2.1
	100 m	2.3	3.1	2.3	3.1	2.2
S400	Track	3.4	4.8	3.5	4.6	3.3
	70 m	3.6	5.0	3.4	4.9	3.4

There is also an interesting finding when we compare TL with TL difference plots. At less TL regions, the TL differences appear to be smaller than at other locations.

5. Three-Dimensional Modal Analysis

From the TL results presented in the previous section, we have seen the importance of 3D effects in this region of interest. In this section, we apply MOS3DPEF, a 3D modal analysis based on 3D PE field computations[15–17] to investigate the 3D effects on modal propagation induced by variations in the water column and bathymetry.

Using a similar method, we reconstructed the sound speed profiles at 19:40 and 22:10 on May 5 according to the satellite image shown in Fig. 2, in which an internal wave crest is clearly displayed.

From the simulated PE sound fields for deep and shallow region using modal sources, we calculated the modal spectrum and assembled the mode coupling matrices. We used modes 1–10 to be the exciting modes and computed the modal spectrum also on modes 1–10. In mode coupling matrices, each small block corresponds to a combination of a specific start mode and an output mode. The horizontal axis (left to right) in each small block is clockwise azimuth, and the vertical axis (top to bottom) is range from source location. The correspondence between the environment and the modal results is detailed in the Appendix.

For deep source case, as shown in Fig. 1, the event at 19:40 represented a background where the nonlinear internal wave crest just arrived the source location but has not entered the region of interest; the event at 22:10 represented a situation where the nonlinear internal wave crest has entered the region and propagated halfway on the acoustic propagation track. Two frequencies, 224 and 400 Hz, were used in our calculation. In Fig. 5, we plot the mode coupling matrices with deep source: (a) of background case at frequency of 224 Hz; (b) of nonlinear internal wave crest propagated halfway on the track at frequency of 224 Hz; (c) of background case at frequency of 400 Hz; (d) of nonlinear internal wave crest propagated to halfway on the track at frequency of 400 Hz. In Figs. 5(b) and 5(d), the diagonal blocks show that the wave crest causes severe horizontal refraction for all modes. The lines in the blocks sketch the locations of the nonlinear internal wave crest. One interesting point is that the modal coupling effect is reduced when the nonlinear internal wave crest is in the track comparing Figs. 5(b) to 5(a) and 5(d) to 5(c), respectively.

For the shallow source case, the event at 19:40 represented a background where the nonlinear internal wave crest was still away from the source location; the event at 22:10 represented a situation where the nonlinear internal wave crest just entered the region. Two frequencies, 300 and 400 Hz, were used in our calculation. In Fig. 6, we plot the mode coupling matrices with the shallow source: (a) for the background case at frequency of 300 Hz; (b) when the nonlinear internal wave crest propagated just into the track at frequency of 300 Hz; (c) for the background case at frequency of 400 Hz; (d) when the nonlinear internal wave crest propagated just into the track at frequency of 400 Hz. The shallow source cases are of a different nature from the deep source cases. The acoustic tracks in shallow source cases are almost along isobath or slightly oblique from isobath so that

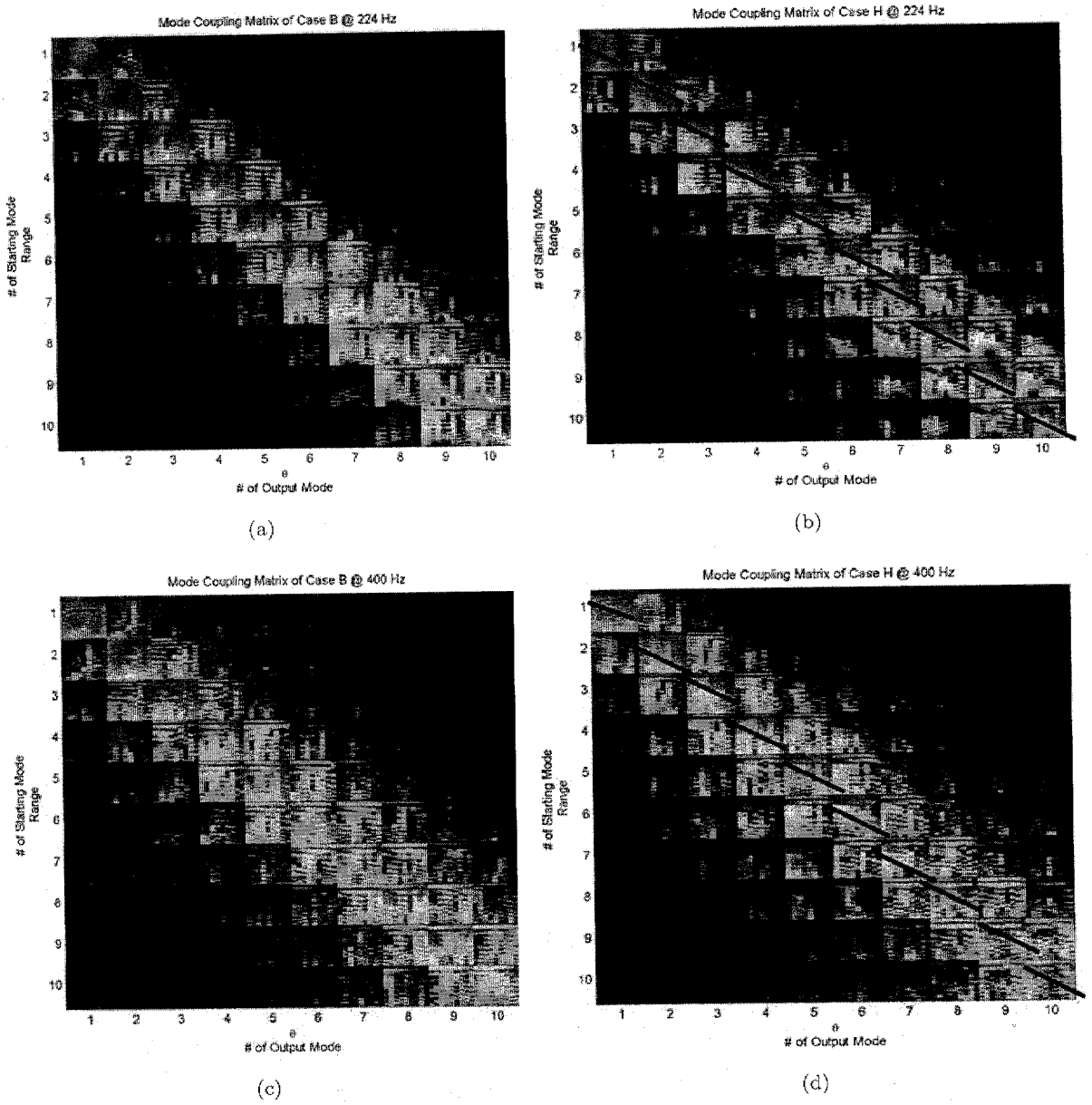

Fig. 5. Mode coupling matrices with deep source (a) of background case at frequency of 224 Hz; (b) of nonlinear internal wave crest propagates halfway on the track at frequency of 224 Hz; (c) of background case at frequency of 400 Hz; (d) of nonlinear internal wave crest propagates halfway on the track at frequency of 400 Hz.

the modal energies refract toward deeper regions. In other words, the 3D effects due to bathymetry are the dominant factor in shallow source cases.

6. Concluding Remarks

In this paper, a 3D ocean environment at the ASIAEX SCS site was reconstructed. We investigated 3D acoustic effects in this reconstructed environment by looking at the TL

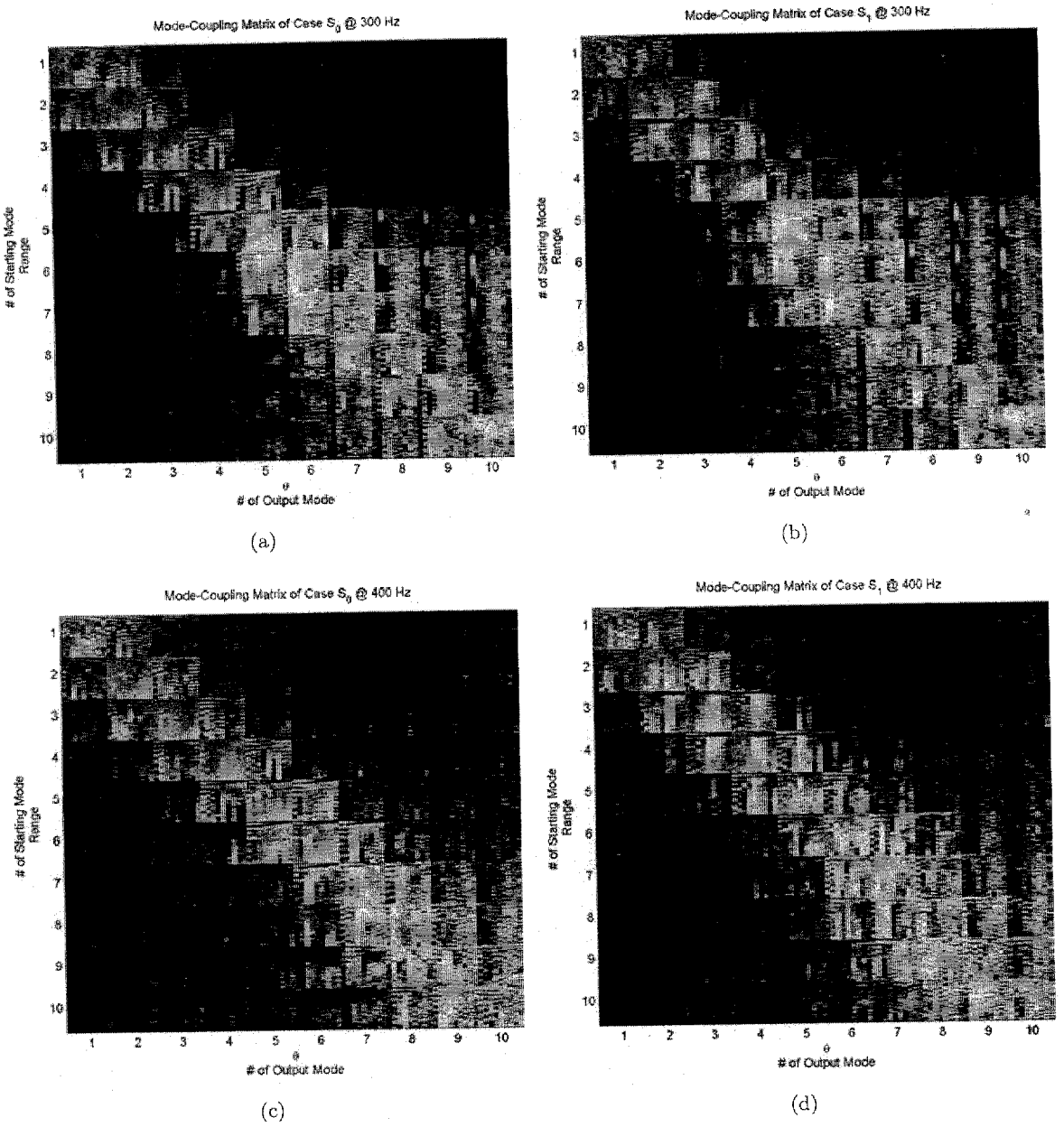

Fig. 6. Mode coupling matrices with shallow source (a) of background case at frequency of 300 Hz; (b) of nonlinear internal wave crest propagates just into the track at frequency of 300 Hz; (c) of background case at frequency of 400 Hz; (d) of nonlinear internal wave crest propagates just into the track at frequency of 400 Hz.

results plus modal analysis and comparison among several characteristic cases. The 3D effects are found to be more important in shallow water when viewed from the results of the variation in bottom topography or water column properties. The presented three sound speed profiles contributed 3D effects of the same order. However, the existence of changes in the water column and the coupling with the bathymetry obviously affected the distribution

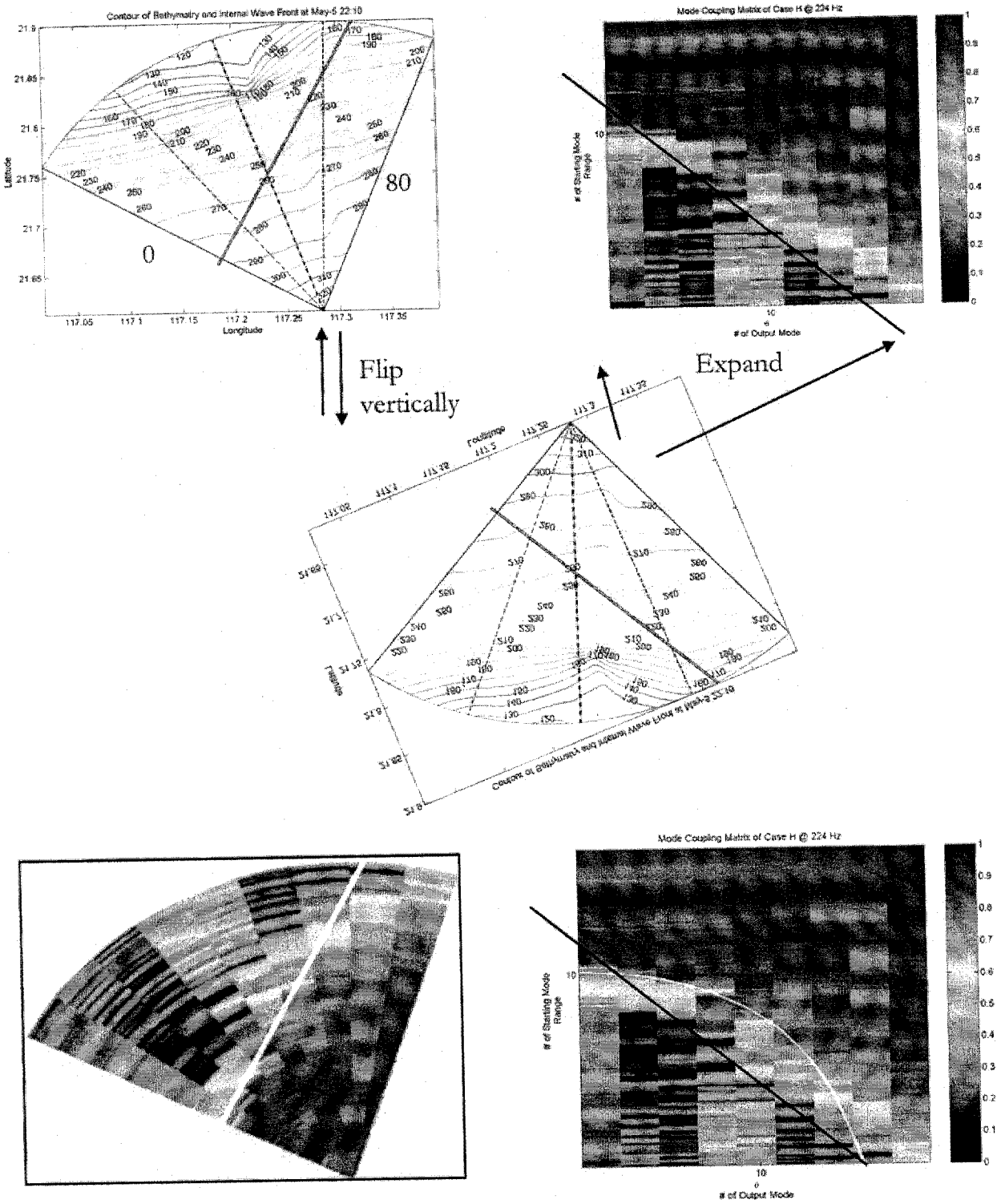

Fig. A.1. Schematic of the correspondence between each block in the modal analysis of numerical results and the ocean environment. Note that the white line in left image becomes the white secant curve on the right.

of the 3D effects. Under such consideration, sound fields of higher frequency give larger difference values, whereas in shallow case the differences are even larger. The 3D computed TL results were presented as well to show the influences of (a) the internal tide coupled with bathymetry, (b) the nonlinear internal waves coupled with bathymetry, and (c) bathymetry solely with mean profiles. From the 3D modal spectrum analysis, we found strong scattering of mode energy by the variations in water column, especially in higher modes and at higher frequencies. In summary, the nonlinear internal wave crest causes severe horizontal refract for modal propagation.

It is of interests to have 3D calculations compared with experimentally measured acoustic data from this computational region in the future, which has not been done in this part of research.

Acknowledgment

The authors are very grateful to Dr Ding Lee and Prof. James Lynch for their insightful comments. The authors are also indebted to the ASIAEX team's great achievement in making a successful experiment. The work is supported by the National Science Council of Taiwan under project No. 92-2611-E-002-005-CCS.

Appendix

Here we give the detail of the correspondence between the environment and the modal results. Understanding of this relation will clearly reveal the effects on acoustics due to the variations in the environment.

Figure A.1 schematically explains how each small block in the modal analysis of numerical results corresponds to the ocean environment. Take the deep region as an example, first flip the region vertically relative to the source location as the center to make the source appear at the top and the zero azimuth placed at left. Then expand the fan-like region to a rectangle. Now one has the same axes as in each small block of mode coupling matrix. As an example, in Fig. A.1 the black line crossing the region represents the nonlinear internal wave crest, accordingly we can distinctly see that the mode energy was strongly scattered by the nonlinear internal wave. (Also note that the white line in left image showing the nonlinear internal wave location should become a white secant curve in the right when the polar coordinates are "unwrapped".)

References

1. D. Lee and M. H. Schultz, *Numerical Ocean Acoustic Propagation in Three Dimensions* (World Scientific, Singapore, 1995), pp. 138–144.
2. G. Botseas, D. Lee and D. King, FOR3D: A computer model for solving the LSS three-dimensional wide angle wave equation, NUSC Technical Report 7993, Naval Underwater Systems Center, New London, CT, USA (1987).
3. A. Tolstoy, 3-D Propagation issues and models, *J. Comput. Acoust.* **4**(3) (1996) 243–271.

4. R. Oba and S. Finette, Acoustic propagation through anisotropic internal wave fields: Transmission loss, cross-range coherence, and horizontal refraction, *J. Acoust. Soc. Am.* **111**(2) (2002) 769–784.
5. S. Finette and R. Oba, Horizontal array beamforming in an azimuthally anisotropic internal wave field, *J. Acoust. Soc. Am.* **114** (2003) 131–144.
6. K. B. Smith, C. W. Miller, A. F. D'Agostino *et al.*, Three-dimensional propagation effects near the mid-Atlantic Bight shelf break (L), *J. Acoust. Soc. Am.* **112**(2) (2002) 373–376.
7. C.-F. Chen and J.-J. Lin, Three dimensional effect on acoustic transmission in Taiwan's Northeastern Sea, in *Proc. Int. Shallow-Water Acoustics*, Beijing (1997).
8. C.-F. Chen, J.-J. Lin and T. Lee, Acoustic transmission of Taiwan's northeast sea, *Acta Oceanogr. Taiwanica* **34** (1995) 39–51.
9. B. G. Katsnel'son and S. A. Pereselkov, Low-frequency horizontal acoustic refraction caused by internal wave solitons in a shallow sea, *Acoust. Phys.* **46** (2000) 684–691.
10. B. G. Katsnel'son and S. A. Pereselkov, Space-Frequency dependence of the horizontal structure of a sound field in the presence of intense internal waves, *Acoust. Phys.* **50** (2004) 169–176.
11. A. R. Robison and D. Lee, *Oceanography and Acoustics — Prediction and Propagation Models* (AIP Press, New York, 1994).
12. A. Newhall, L. Costello, T. Duda *et al.*, Preliminary acoustic and oceanographic observations from the ASIAEX 2001 South China Sea experiment, WHOI Technical Report WHOI-2001-12, Woods Hole Oceanog. Inst., Woods Hole, Massachusetts, USA (2001).
13. A. A.-K. Liu, Nonlinear internal waves in the South China Sea during ASIAEX, NTU Technical Report UAL-NTU-TR 0302, Natl. Taiwan Univ., Taipei, Taiwan (2003).
14. D. Lee, A. D. Pierce and E.-C. Shang, Parabolic equation development in the twentieth century, *J. Comput. Acoust.* **8**(4) (2000) 527–637.
15. E.-C. Shang and Y.-Y. Wang, Acoustic travel time computation based on PE solution, *J. Comput. Acoust.* **7**(1) (1991) 91–100.
16. P.-S. Chen and C.-F. Chen, Study of the effect of topography and fronts on the acoustic modal propagation, in *First Symposium on Underwater Technology of Republic of China*, Taipei, Taiwan (1998).
17. P.-S. Chen, Three-dimensional modal analysis of underwater acoustic propagation in the ocean, Master thesis, Department of Naval Architecture and Ocean Engineering, National Taiwan University, Taiwan (1998).